Lab on a Chip

Accepted Manuscript

ROYAL SOCIETY OF CHEMISTRY

www.rsc.org/loc

Multiphase Optofluidics on an Electro-Microfluidic Platform Powered with Electrowetting and Dielectrophoresis

Shih-Kang Fan[a*] and Fu-Min Wang[b]

[a]Department of Mechanical Engineering, National Taiwan University, Taipei, Taiwan.
[*]E-mail: skfan@fan-tasy.org; Tel: +886-2-33664515; Fax: +886-2-23631755; Address: No. 1, Sec. 4, Roosevelt Road, Taipei 10617, Taiwan
[b]Graduate Institute of Electronic Engineering, National Taiwan University, Taipei, Taiwan.

Shih-Kang Fan received his B.S. degree from National Central University, Taiwan, in 1996, and his M.S. and Ph.D. degrees from UCLA in 2001 and 2003, respectively. Between 2004 and 2012, he was with the Institute of Nanotechnology and Department of Material Sciences and Engineering at National Chiao Tung University, Taiwan. He is now an Associate Professor of Mechanical Engineering at National Taiwan University, Taiwan. Dr. Fan is the recipient of several prestigious young investigator awards in Taiwan, including National Science Council Ta-You Wu Memorial Award and Academia Sinica Research Award for Junior Research Investigators. His research interest focuses on electro-microfluidics.

Fu-Min Wang received the B.S. (1993) and M.S. (1995) in Mechanical Engineering from National Taiwan University. He received the M.S. (2000) at UCLA and Engineer's Degree (2007), working on two-phase transport phenomena in the microchannel for Proton Exchange Membrane (PEM) fuel-cell applications, at Stanford University. He was a research technical expert at National Taiwan

University and worked on microfluidics, electron beam lithography from low to high voltages, low-temperature scanning electron microscopy, and focused ion beam for both semiconductors and biomedical applications. He is interested in exploring, learning and educating advanced science and technology in inspiring ways.

ABSTRACT

For diverse material phases used on an electro-microfluidic (EMF) platform, exploiting the electro-optical properties of matter in varied phases is essential to reap the benefits of the optofluidic capabilities of that platform. Materials in the four fundamental phases – solid-phase dielectric layer, liquid-phase droplet, gas-phase bubble, and plasma-phase bubble microplasma – have been investigated to offer electrically tunable optical characteristics for the manipulation of fluids on an EMF platform. Here we present an overview of the basic driving mechanisms of electrowetting and dielectrophoresis on the EMF platform. Three optofluidic examples occurring in multiple phases are described: solid optofluidics -- liquid and light regulation with electrowetting on a solid polymer dispersed liquid crystal (PDLC) dielectric layer, liquid optofluidics -- transmittance and reflectance modulation with formation of a particle chain in a liquid droplet, and gas and plasma optofluidics -- ignition and manipulation of a bubble microplasma with liquid dielectrophoresis. On combining the various materials possessing diverse electro-optical characteristics in separate phases, the EMF platform becomes an ideal platform for integrated optofluidics.

Introduction

Optofluidics combines and integrates optics and fluidics to produce versatile systems that are achievable only with difficulty through either field alone. With the spatial and temporal control of the microfluids, the optical properties can be varied, providing highly flexible, tunable, and reconfigurable optical systems. Since the emergence of optofluidics, numerous systems with varied configurations[1,2] have been developed and applied to imaging[3], light routing[4-6], bio-sensors[7], energy[8,9], and other fields[10-12]. Among these optofluidic systems, the unique optofluidic characteristics were generated by the solid-liquid and liquid-liquid interactions when microfluids were continuously pumped along microchannels.

Alternatively, manipulation of discrete microfluids, e.g., droplets, has also been intensively investigated for diverse applications including optics. A droplet behaves as an independent liquid compartment in which a chemical reaction, biological synthesis, and optical pumping can occur.[13-15] On a digital (droplet-based) electro-microfluidic (EMF) platform, instead of continuously flowing along the stream, droplets are individually manipulated between two parallel plates using electrowetting and dielectrophoresis[16-18] for applications in chemistry, biology, and medicine[19-21]. The diversity of liquids has led EMF to optical, electrical, and thermal applications commensurate with their corresponding physical properties. In optical applications, droplet-based lenses[22-24], mirrors[25], prisms[26-28], and reflective electronic paper displays[29,30] have been devised on controlling the surface profile or the position of a droplet possessing appropriate optical properties, including the refractive index, transmittance and color.

Here we depict several optofluidic characteristics enriched with varied methods that exploit the four fundamental phases of matter on an EMF platform.

Accompanying the manipulation of a liquid by electrowetting and dielectrophoresis, the optical properties of various materials in the four basic phases -- including solid (polymer dispersed liquid crystal dielectric), liquid (particle suspension droplet), gas (air or inert gas bubble), and even plasma phases -- are electrically programmed on the parallel-plate EMF platform. Various important parameters are specified throughout the article to illustrate the diverse but related phenomena on the EMF platform.

EMF by Electrowetting

Electrowetting is an electrical means of varying the apparent contact angle of a liquid droplet on a solid surface[31,32]. The variation of contact angle is commonly studied with a sessile drop placed on a bottom electrode coated with a dielectric layer and a hydrophobic (e.g., Teflon) layer as shown in Fig. 1(a). On applying voltage V between the insulated bottom electrode and a Teflon-coated probe immersed in the liquid droplet, the contact angle of the droplet alters from θ_0 to $\theta(V)$, as expressed with the Lippmann-Young equation[33-35]:

$$\cos\theta(V) = \cos\theta_0 + \frac{\varepsilon_0 \varepsilon_D}{2\gamma_{LG} t} V_D^{\,2}, \qquad (1)$$

in which ε_0 (8.85×10^{-12} F/m) denotes the permittivity of vacuum, ε_D the relative permittivity of the dielectric layer of thickness t, γ_{LG} the liquid-gas interfacial tension and V_D the voltage drop across the dielectric layer. Because the electrowetting under discussion here occurs on a dielectric layer, the phenomenon is named also electrowetting-on-dielectric (EWOD). Ratio V_D/V varies with the applied frequency and the properties of the employed liquid and solid materials[36,37]. A simplified equivalent circuit of the liquid droplet comprises a resistor and a capacitor in parallel either in an open surface device (Fig. 1(b)) or in a parallel-plate device (Fig. 1(c)). In

general, ratio V_D/V increases as the applied frequency decreases. To drive droplets by electrowetting, a DC or a low-frequency AC electric signal is typically applied. When evaluating the electrowetting of a sessile drop immersed in an immiscible fluid medium such as oil, the liquid-gas interfacial tension γ_{LG} in Eq. (1) becomes replaced with liquid-medium interfacial tension γ_{LM}. Because electrowetting varies the contact angle reversibly on application of a voltage, it has been developed for several optical components, including liquid lenses[22-24], prisms[26-28], and displays[29,30]. On adjusting the contact angle of a droplet, its curvature varies accordingly and refracts the incident light to achieve a liquid lens with a tunable focal length. The applied voltage modulates the projected area of the droplet, thus distinguishing bright and dark states to realize a reflective electronic paper display.

In this review, we describe several optofluidic applications on an EMF platform in which fluids are driven between parallel plates. As shown in Fig. 1(d), with patterned electrodes on the bottom plate, V_D generates electrowetting and causes uneven contact angles and curvatures of the droplet on its two sides. According to the Laplace-Young equation[33], the uneven radii of curvature (e.g., r_L and r_R in Fig. 1(d)) generate a difference of liquid pressure between the two sides and pump the droplet toward the activated electrode. In addition to electrowetting, dielectrophoresis provided by V_L is described subsequently for manipulation of a particle suspended in droplets, dielectric droplets and bubbles. As shown in Fig. 1(d), materials in three phases are found in the EMF platform, including solid plates, liquid droplets and air environment. With a microplasma demonstrated on the EMF platform, the four fundamental phases are available on the platform to enhance its optofluidic performance. In the following sections, solid, liquid, gas, and plasma-phase optofluidics are demonstrated. Throughout the article, we introduce varied phenomena on the EMF platform with a similar parallel-plate configuration. In

general, for purposes of observation, the top plate has a transparent electrode coated with a hydrophobic surface. For reasons of manipulation, the bottom plate contains appropriately designed electrode patterns covered with a dielectric layer and a hydrophobic surface.

Solid Optofluidics: PDLC Dielectric

As described in Eq. (1), the dielectric layer between a solid electrode and a liquid is essential for electrowetting; the dielectric material is generally chosen to decrease the driving voltage and to enhance the performance of electrowetting. Using a dielectric layer with appropriate electro-optical effects would improve the optofluidic characteristics of the EMF platform. A polymer dispersed liquid crystal (PDLC)[38], possessing both insulating and electro-optical properties, serves as a dielectric layer of electrowetting to generate simultaneously modulated contact angle and transmittance on application of a voltage[39]. As shown in Fig. 2(a), the PDLC consists of LC droplets of micrometer size dispersed in solidified polymer matrices. Before application of a voltage, the orientation of the directors (long axes) of the LC molecules, shown as solid lines in the LC droplets, is random. For a LC with a large birefringence, the difference of the refractive indices between the random LC droplets and the polymer is significant, which strongly scatters incident light and decreases the transmittance of the PDLC. As shown in Fig. 2(b), when sufficient voltage is applied, the directors of the LC droplets covered with the water droplet become reoriented parallel to the direction of the electric field. If the ordinary refractive index of the LC matches that of the polymer, the PDLC becomes isotropic and highly transparent; voltage V_D across the dielectric layer concurrently contributes to the electrowetting. A polydimethylsiloxane (PDMS) layer (thickness 10 μm) containing (8.3 mass %)

dispersed LC (E7) droplets (average diameter 3 μm) was spun and cured on a glass plate (thickness 0.7 mm) coated with transparent indium tin oxide (ITO, thickness 100 nm). A Teflon layer (thickness 50 nm) was then coated on top of the PDLC layer. Figures 2(c) and 2(d) show a basic liquid lens with coupled electrowetting and electro-optical effects of the PDLC. On selecting carefully the LC and polymer materials, the difference of the refractive indices between random LC droplets and the polymer becomes significant, which scatters incident light and renders a small transmittance without application of a voltage, as the blurred and dim background image shown in Fig. 2(c). With a voltage applied, the contact angle of the water droplet decreases while the directors of the LC droplets in the electric field become reoriented. When the refractive index of the aligned LC matches that of the polymer, the incident light passes through the PDLC film, making it more transparent. Hence, the focal length of the liquid lens and the amount of light passing through the liquid lens are both modulated with the applied voltage. As shown in Fig. 2(d), the background image with letters passing through the water droplet became clear and magnified. PDLC can undoubtedly be embedded also into current electrowetting-based electronic-paper displays to enhance the contrast ratio on modulating both the conformation of the dye droplet and the transmittance of the dielectric layer.

Various fluidic functions, including droplet transport, splitting, and merging, have been demonstrated using PDLC as a dielectric layer. As shown in Fig. 2(e), the bottom plate contains five patterned driving electrodes (1 mm × 1 mm) covered with PDLC dielectric and Teflon hydrophobic layers. When applying a voltage between the top blank electrode and the bottom driving electrode(s), electrowetting occurs and drives the water droplet. The direction of the LC droplets in the electric field simultaneously aligns with the electric field and provides bright regions as shown in

the top view of Fig. 2(e). As the water droplets move forward, the bright regions increase until the water droplets move entirely onto the powered electrodes. Figure 2(f)-2(i) show the moving and splitting of a water droplet (volume 0.75 μL) between the parallel plates (spacing 300 μm) on applying 1 kHz and 100 V_{RMS}. The bright regions were the overlapping areas of water droplets and the powered bottom electrodes indicated with arrow signs on the figures. The droplet became dim after removal of the applied voltage as shown in Fig. 2(g).

Liquid Optofluidics: Particle Droplets

Like solid PDLC participants in optofluidics, a water droplet can be modified to achieve additional electro-optical phenomena; for example, adding addressable neutral particles to the water droplets to become particle suspension droplets or colloidal droplets. As mentioned above, low-frequency signals provide V_D that generates electrowetting to drive the droplets and even to reorient the LC molecules within the PDLC layer in the parallel-plate EMF platform. On increasing the frequency, a greater voltage is consumed in the liquid droplet, shown as V_L in Fig. 1(c). Ratio V_L/V depends on frequency as expressed in[37]

$$V_L / V = \mathrm{Re}\left(\frac{j2\pi f C_D R_L}{1 + j2\pi f (C_D + C_L) R_L} \right), \quad (2)$$

in which R_L, C_L and C_D denote the equivalent resistance and capacitances of the liquid and dielectric as shown in Fig. 1(c). Although V_L contributes no electrowetting, it establishes an electric field, V_L/d, that would polarize the particles and cells suspended in the liquid droplet. When the electric field is non-uniform, it actuates the polarized particles by dielectrophoresis (DEP)[40-42]. The dielectrophoretic force, F_{DEP}, exerted on a spherical particle of radius a by dielectrophoresis is described with

$$F_{DEP} = 2\pi a^3 \varepsilon_L \mathrm{Re}\left(\frac{\varepsilon_P^* - \varepsilon_L^*}{\varepsilon_P^* + 2\varepsilon_L^*}\right)\nabla E^2 , \quad (3)$$

in which E denotes electric field, ε^*_P and ε^*_L are the complex permittivities of the manipulated particles and of the suspension liquid, respectively, which depend on frequency, expressed as

$$\varepsilon^*_{P,L} = \varepsilon_0 \varepsilon_{P,L} - j\frac{\sigma_{P,L}}{2\pi f}, \quad (4)$$

in which $\varepsilon_{P,L}$ is the relative permittivity and $\sigma_{P,L}$ the conductivity of the particle ($_P$) or the suspension liquid ($_L$); f is the frequency of the electric field.

With appropriate frequencies, V_D and V_L are selectively applied to actuate droplets on a mm scale and particles or cells on a μm scale, respectively, realizing a droplet-based concentrator of particles or cells based on the cross-scale manipulating abilities of the EMF platform[37]. Figure 3(a) shows lines of the electric field in a droplet on applying a high-frequency voltage (V_{HF}) between the top electrode and one bottom square driving electrode in a parallel-plate device. To achieve a concentration of particles in the droplet by dielectrophoresis, creating a non-uniform electric field by the shrunk electrodes (Fig. 3(b)) is necessary. As shown in Fig. 3(c), 3(h), and 3(l), a droplet (volume 0.5 μL) was dispensed in an immiscible filler fluid of silicone oil (viscosity 50 cSt) between parallel plates (spacing 200 μm). The top plate contained a blank ITO electrode coated with a thin hydrophobic layer; the bottom plate contained eight strip electrodes (100 μm × 1.6 mm) at the centre and two square electrodes (1 mm × 1 mm) on each side, all made of Au/Cr and covered with dielectric (SU-8, thickness 5 μm) and hydrophobic (Teflon, thickness 50 nm) layers. A high-frequency voltage (V_{HF}, 2 MHz and 60 V_{RMS}) was applied to the strip electrodes sequentially to generate non-uniform electric fields to drive mammalian Neuro-2a cells (Fig. 3(h)-3(k)) and polystyrene particles (diameter 5 μm, Fig. 3(l) and 3(m)) from left to

right by positive and negative dielectrophoresis, respectively. The cells were originally suspended in a solution (3% PBS and 280 mM isotonic sucrose, concentration 8.6 × 10^5 cells/mL), while particles were dispersed in water (concentration 1.4 × 10^8 particles/mL). The droplet was split on applying low-frequency voltages (V_{LF}, 1 kHz and 80 V_{RMS}) into two droplets with distinct particle concentrations, as shown in Fig. 3(k) and 3(m).

In the application to concentrating cells or particles, V_{HF} concentrates the suspended cells and particles on moving them laterally with non-uniform electric fields. Instead of the lateral movements, applying V_{HF} between the top and bottom blank electrodes alternatively generates a uniform electric field (Fig. 4(a)) to polarize the particles. These polarized particles are further moved by a dipole-dipole interaction to form particle chains along the electric field lines as shown in Fig. 4(b)[43,44]. Formation of the particle chains results in a large variation of optical transmittance and reflectance of the droplet. As shown in Fig. 4(c) and 4(d), a water droplet containing polystyrene particles (diameter 5 μm, concentration 1.4×10^8 particles/mL) was placed between parallel plates (spacing 100 μm) coated with electrode (ITO), dielectric (SU-8, thickness 5 μm) and hydrophobic (Teflon, thickness 50 nm) layers[43]. Before application of a voltage, the particles were evenly dispersed, scattered incident light, and displayed as a dark droplet as shown in Fig. 4(c). When V_{HF} (200 kHz and 28 V_{RMS}) was applied, the AC electric field (0.28 MV m^{-1}) polarized the particles and formed particle chains along the lines of the electric field to display a relatively transmissive or reflective droplet on a high reflectance background as shown in Fig. 4(d). A bright droplet was obtained because the white background behind the EMF platform reflected the incident light. In addition to manipulating particles on a μm scale, electrowetting was also investigated to drive the suspension droplets on a mm scale. The pumping of a droplet with tunable

transmittance and reflectance was examined in the EMF platform as shown in Fig. 4(e). On applying appropriate electric signals, the droplet and the suspended particles were selectively driven. Again, electrowetting requires a voltage across the dielectric layer V_D when applying V_{LF}, while the particle polarization needs an electric field inside the liquid V_L when applying V_{HF}. Tuning the frequency of the electric signal effectively determines the desired phenomenon occurring on the EMF platform. When V_{LF} (1 kHz and 50 V_{RMS}) was applied between the parallel plates (spacing 100 μm), most of the applied voltage dropped across the dielectric layer to generate electrowetting and to actuate the droplet (volume 0.1 μL) on a mm scale (Fig. 4(f)). In contrast, on applying V_{HF} (200 kHz and 50 V_{RMS}), most voltage established an electric field in the liquid to manipulate the particles on a μm scale and to alter the transmittance and reflectance of the droplet (Fig. 4(g)). The variation of transmittance and reflectance might be applied to analyze the properties of functional particles or bio-particles, i.e., cells, proteins and DNA, according to the variation of transmittance.

Based on the study of particle manipulation in a moving droplet described above, a display medium associated with electronic paper was developed using a simple suspension of uncharged neutral particles in water[44]. Electronic paper is a paper-like display pursuing the goals of being reflective, flexible, bendable, portable, bistable and energy-saving[29,30,45]. The mechanisms of actuation (e.g., electrowetting[29,30] and electrophoresis[45]) and materials (e.g., liquids and particles) found in many electronic-paper displays are also commonly investigated in the field of microfluidics. Electronic paper can hence be regarded as a promising example of optofluidics that applies microfluidics to achieve optical effects. A particle-based electronic-paper display provides a large reflectance at a cost smaller than that of other techniques. The dyed particles strongly reflect incident light and display saturated colors. Particle suspensions are, moreover, suitable for the development of bendable and flexible

displays because a slight alteration of the thickness of the suspension has no influence on the display performance, unlike liquid crystal displays that typically require a precise and fixed thickness.

The particle suspension droplet was then developed as a low cost display medium[44]. The particle chains, formed out of plane and parallel to the electric field lines, decrease the planar density of particles and greatly alter the transmittance and reflectance of the display medium to provide bright and dark states. Devices with electrodes of two designs, directly driven electrodes and arrayed electrodes shown in Fig. 4(h), were tested. As shown in Fig. 4(i) and 4(j), suspensions of blue and red polystyrene particles (diameter 3 μm, concentration 1.68×10^9 particles/mL) were packaged between parallel plates a gap (spacing 100 μm). When 500 kHz and 48 V_{RMS} (electric field 0.48 MV m^{-1}) was applied between the top blank and bottom patterned electrodes covered with an appropriate dielectric (SU-8, thickness 1 μm) and hydrophobic (Teflon, thickness 55 nm) layers, the particles in the electric field region became polarized to form particle chains. These chains altered the transmittance and reflectance of the particle suspension to display an image of the directly driven electrode patterns, 'NCTU CPT' that was observed from the normal and tilt angle 70° as shown in Fig. 4(i) and 4(j), respectively. Figure 4(k) shows another design of a device with 5 × 5 arrayed electrodes containing segmented suspensions of black polystyrene particles (diameter 3 μm, concentration 1.68×10^9 particles/mL) with no voltage applied. Each compartment of this suspension represented a display pixel of size 2 mm × 2 mm × 100 μm. Programmable images were demonstrated using 500 kHz and 9 V_{RMS} (electric field 0.09 MV m^{-1}) as shown in Fig. 4(l) and 4(m).

Gas and Plasma Optofluidics: Bubble Microplasma

After describing two examples of exploiting the electro-optical properties of the solid-phase dielectric and liquid-phase droplet with V_D (with V_{LF} applied) and V_L (V_{HF} applied), respectively, we proceed to illustrate gas and plasma-phase optofluidics on the EMF platform. Air bubbles become reversely driven in water with electrowetting[46,47] on the EMF platform. As droplets provide a convenient means to handle various liquids with precise volumes, bubbles facilitate a quantitative preparation of gas samples for a gaseous lab-on-a-chip, but actuating bubbles in an aqueous medium might alter the composition of the bubbles because of the large vapor pressure of water (23.8 torr at 25°C), which can be as much as 10^9 times that of oil (e.g., 10^{-8} torr for some oils for vacuum pumps). To realize gaseous digital (now bubble-based) EMF for reproducible analysis of gaseous samples, an inert and stable medium as an environment to manipulate bubbles is necessary. Driving bubbles in an oil medium of small vapor pressure was thus necessary[48]. Because electrowetting cannot drive dielectric liquid droplets on varying the contact angle, liquid dielectrophoresis was applied to actuate oil droplets and to drive bubbles in an oil medium.

Dielectrophoresis not only provides body forces on suspended objects of interest, as described above (Fig. 3 and 4), but also supplies surface forces to draw bulk liquids, including dielectric ones, of greater relative permittivity into a region of strong electric field of smaller relative permittivity (air)[49,50]. As illustrated in Fig. 5(a), when voltage V is applied between parallel electrodes (width W, spacing d), a dielectric droplet is attracted toward the region of strong electric field with a dielectrophoretic force[18],

$$F_{DEP} = \frac{\varepsilon_0 (\varepsilon_L - 1) W}{2d} V^2, \quad (5)$$

in which ε_L is the relative permittivity of the liquid. In this analysis, because the electrodes contact the droplet directly, V_L equals V. Droplets of decane, hexadecane and silicone oil were transported between parallel plates on application of a sufficient DC voltage on the electrodes (Cu/Cr) covered only with hydrophobic (Teflon, thickness 50 nm) layers without dielectric layers[18]. A silicone oil droplet (viscosity 20 cSt, volume 0.15 μL) was split (Fig. 5(b) and 5(c)), transported, and merged on applying 420 V_{DC} between parallel plates (spacing 75 μm). With the ability to actuate oil droplets, local optical properties, such as refractive index and colour, are switchable. The optofluidic components with aqueous droplets[22-30] can thus be implemented with more stable and non-volatile oil droplets. For example, oil immersion is a widely used technique to increase the resolution of a microscope; an oil-droplet lens of variable focus has been developed[51].

On applying a dielectric layer (SU-8, thickness 1 μm) to the driving electrodes of the parallel-plate device, both dielectric and conductive droplets are addressable. As shown in Fig. 5(d), dielectrophoresis and electrowetting are selectively generated on applying varied signals on the same dielectric-covered electrodes to drive silicone oil and water droplets, respectively. Concurrently transporting silicone oil and water droplets along an electrode loop, merging water and oil droplets, and transporting the merged water-in-oil (W/O) encapsulated droplet were performed[18]. Two silicone oil (viscosity 20 cSt, volume 25 nL) and water droplets were first placed on an electrode loop comprising 12 square driving electrodes (1 mm × 1 mm) between parallel plates (spacing 25 μm). The upper oil droplet in Fig. 5(e) was driven by dielectrophoresis with 260 V_{DC} (V_{DEP}), whereas the lower water droplet was moved on electrowetting with a sinusoidal wave signal (V_{EWOD}, 1 kHz and 34 V_{RMS}). Once again, V_{DEP} generated V_L to actuate the oil droplets, whereas V_{EWOD} provided V_D to pump the water droplets. When the oil droplet touched the water droplet, the oil immediately

surrounded the water droplet to form a encapsulated droplet (1:1 W/O) with a structure of water core and oil shell as shown in Fig. 5(f). An encapsulated droplet should find special optofluidic applications because it holds two liquids with distinct optical properties (e.g., refractive index) and two adjustable interfaces between water and oil and between oil and air. In general lab-on-a-chip applications, the benefits of an encapsulated droplet as a technique are to enhance fluidic manipulation, to decrease biofouling, to decrease evaporation and to simplify device packaging. Encapsulated droplets with metered and removable oil shells were also achieved[52]. As shown in Fig. 5(g), between parallel plates (spacing 25 μm), a non-volatile silicone oil droplet (viscosity10 cSt, volume 2.5 nL) was created on applying 240 V_{DC} to the driving electrodes (316 μm × 316 μm), while a water droplet (volume 25 nL) was created on applying 1 kHz and 48 V_{RMS} to the electrodes (1 mm × 1 mm). SU-8 (thickness 1.1 μm) served as the dielectric layer; Teflon (thickness 55 nm) was applied as the hydrophobic surface. Merging resulted in an encapsulated droplet (10:1 W/O, Fig. 5(h)). Encapsulated droplets with varied volume ratios of water to oil were readily obtained on merging water and oil droplets of desired numbers. The oil shell was removed on dissolving silicone oil in a non-polar solvent, hexane, which is immiscible with water (Fig. 5(i)). The water droplet subsequently emerged from hexane. A thin hexane shell rapidly evaporated to restore the original bare water droplet, as shown in Fig. 5(j).

With the ability to drive droplets of silicone oil in air by dielectrophoresis, the manipulation of gas bubbles in an inert silicone oil environment becomes possible[48,53]. As shown in Fig. 6(a) and 6(b), bubbles were manipulated between parallel plates (spacing 50 μm) filled with silicone oil (viscosity 20 cSt) with electrodes covered with a dielectric layer (SU-8, thickness 1.8 μm)[53]. Large reservoir electrodes were designed to host and to store gaseous samples. Driving electrodes (2 mm × 2 mm)

served to manipulate the bubbles. A surrounding electrode on the bottom plate and a layer of positive photoresist (AZ P4620, thickness 10 μm) on the top plate were designed to have the same shape to confine and to guide bubbles on appropriate driving electrodes. Figure 6(c) and 6(d) show an argon bubble (volume 200 nL) on the left and a helium (volume 200 nL) bubble on the right generated and transported to the centre of the device on applying 2.4 kHz and 315 V_{RMS}. During manipulation of the bubbles, the surrounding electrode was always turned on to maintain the bubble on the driving electrodes. A bubble of the Ar/He mixture was obtained on mixing the two bubbles as shown in Fig. 6(d). The mixed bubble was split into two bubbles (Fig. 6(e)) and the bubble on the right was expelled (Fig. 6(f)). The bubble generation, transport, mixing, splitting, and expulsion facilitate the sample preparation of various bubbles with tunable gaseous composition. The prepared bubble can be further processed and analysed in the following steps, including microplasma ignition.

The dielectrophoretically driven bubbles were further ignited to obtain the fourth phase of matter, plasma, within the bubbles with a dielectric barrier discharge (DBD)[54] at atmospheric pressure and in an inert environment, silicone oil. The plasma provides sufficient energy for a chemical reaction based on excitation, dissociation and ionisation of atoms and molecules. The electronic transition between energy states leads to a characteristic spectral emission that can serve for gas analysis or as a light source. As described above, the bubbles are pushed away from the region of large electric field with dielectrophoresis and positioned at the region of small electric field with no voltage applied. To maintain the position of the bubble during the ignition of the microplasma, a periodic signal of which the voltage is sufficient to ignite the plasma but the power interval is brief enough to prevent bubble movement was therefore applied. When the microplasma was on, the plasma bubble followed the strong electric field as shown in Fig. 6(g). Figure 6(h) and 6(i) demonstrate

microplasma ignition in an Ar bubble with 2.4 kHz and 693 V_{RMS} applied. Before that ignition, a large voltage was applied to the electrodes surrounding the bubble to hold it in place. Once the microplasma was ignited, the surrounding electrodes were turned off to avoid the microplasma splitting. The periodic AC signal was then continuously supplied to sustain the microplasma. The bubble in the plasma phase was positioned with the large electric field, which was the reverse of the driving scheme of the original gas phase; the reason is that the permittivity and conductivity of the bubble alter greatly from the gas phase to the plasma phase. Plasma can be regarded as a conductive fluid containing ions and electrons at large concentrations. As shown in Fig. 6(j) and 6(k), switching the applied signal (2.4 kHz and 655 V_{RMS}) along the driving electrodes transported the microplasma. Splitting the microplasma was demonstrated in Fig. 6(l)-6(n) using 2.4 kHz and 587 V_{RMS}. When the voltage applied on the right bubble was turned off, the microplasma was extinguished. The microplasma was hence ignited, transported, split and extinguished together with the bubble manipulation, all through dielectrophoresis in silicone oil.

Discussion

We demonstrate several examples of optofluidics on the EMF platform. The basic phenomena and parameters are provided in the order solid, liquid, gas, and plasma phases; the optical measurements are not recalled in detail but can be found in the references, such as the transmittance of PDLC[39], the reflectance of particle suspension droplets[43,44] and the optical emission spectra of bubble microplasma[53]. Here we reorganize the phenomena according to the working principles -- electrowetting, particle dielectrophoresis and polarization, and liquid dielectrophoresis as listed in Table 1. Between the parallel plates, electrowetting is

basically caused by V_D, whereas particle and liquid dielectrophoresis are mainly achieved with V_L. From the viewpoint of the manipulated objects, the EMF platform is a general one that drives matter in various phases from liquid to plasma, on varied scales from mm droplet to μm particle, and with diverse conductivity from water to oil. Some experimental examples with parameters, although perhaps not optimum, are provided to show the operating conditions. More detailed information is available in the references[18,37,39,43,44,52,53].

Conclusion

Exploring the electro-optical characteristics of materials in four fundamental phases -- solid, liquid, gas, and plasma -- to improve the optofluidic behaviour on a parallel-plate EMF platform is summarized. First, in the solid phase, PDLC containing tiny LC droplets was integrated in the EMF platform to serve as a dielectric layer providing electrowetting and transmittance modulations. Second, in the liquid phase, droplets having suspended particles were investigated to present dark and bright states that are essential for a display medium on the formation of particle chains in the liquid. Third, in the gas phase, basic bubble functions driven by dielectrophoresis were examined in an inert oil environment. Fourth, in the plasma phase, a microplasma was ignited and handled in dielectrophoretically driven bubbles. Based on current research on multiphase optofluidics on the EMF platform, the integration of materials possessing electrically tunable optical properties or optically modulated electrical characteristics is promising and beneficial for future development of an optical-EMF platform.

References

[1] D. Psaltis, S. R. Quake, and C. Yang, *Nature*, 2006, **442**, 381-386.

[2] V. R. Horowitz, D. D. Awschalom, and S. Pennathur, *Lab Chip*, 2008, **8**, 1856-1863.

[3] X. Heng, D. Erickson, L. R. Baugh, Z. Yaqoob, P. W. Sternberg, D. Psaltis, and C. Yang, *Lab Chip*, 2006, **6**, 1274-1276.

[4] D. B. Wolfe, R. S. Conroy, P. Garstecki, B. T. Mayers, M. A. Fischbach, K. E. Paul, M. Prentiss, and G. M. Whitesides, *Proc. Natl. Acad. Sci. USA*, 2004, **101**, 12434-12438.

[5] Y. Yang, L. K. Chin, J. M. Tsai, D. P. Tsai, N. I. Zheludevd, and A. Q. Liu, *Lab Chip*, 2012, **12**, 3785-3790.

[6] Y. C. Seow, S. P. Lim, and H. P. Lee, *Lab Chip*, 2012, **12**, 3810-3815.

[7] X. Fan and I. M. White, *Nat. Photonics*, 2011, **5**, 591-597.

[8] D. Erickson, D. Sinton, and D. Psaltis, *Nat. Photonics*, 2011, **5**, 583-590.

[9] W. Song and D. Psaltis, *Lab Chip*, 2013, **13**, 2708-2713.

[10] H. Schmidt and A. R. Hawkins, *Nat. Photonics*, 2011, **5**, 598-604

[11] C. Monat, P. Domachuk, and B. J. Eggleton, *Nat. Photonics*, 2007, **1**, 106-114.

[12] Y.-F. Chen, L. Jiang, M. Mancuso, A. Jain, V. Oncescu, and D. Ericckson, *Nanoscale*, 2012, **4**, 4839-4857.

[13] M. T. Guo, A. Rotem, J. A. Heyman, and D. A. Weitz, *Lab Chip*, 2012, **12**, 2146-2155.

[14] S.-Y. Teh, R. Lin, L.-H. Hung, and A. P. Lee, *Lab Chip*, 2008, **8**, 198-220.

[15] S. K. Y. Tang, Z. Li, A. R. Abate, J. J. Agresti, D. A. Weitz, D. Psaltis, and G. M. Whitesides, *Lab Chip*, 2009, **9**, 2767-2771.

[16] M. G. Pollack, R. B. Fair, and A. D. Shenderov, *Appl. Phys. Lett.*, 2000, **77**, 1725-1726.

[17] S. K. Cho, H. Moon and C.-J. Kim, *J. Microelectromech. Syst.*, 2002, **12**, 70-80.

[18] S.-K. Fan, T.-H. Hsien, and D.-Y. Lin, *Lab Chip*, 2009, **9**, 1236-1242.

[19] K. Choi, A. H. C. Ng, R. Fobel, and A. R. Wheeler, *Annu. Rev. Anal. Chem.*, 2013, **5**, 413-440.

[20] M. J. Jebrail, M. S. Bartsch and K. D. Patel, *Lab Chip*, 2012, **12**, 2452-2463.

[21] R. Sista, Z. Hua, P. Thwar, A. Sudarsan, V. Srinivasan, A. Eckhardt, M. Pollack, and V. Pamula, *Lab Chip*, 2008, **8**, 2091-2104.

[22] B. Berge and J. Peseux, *Eur. Phys. J. E*, 2000, **3**, 159-163.

[23] S. Yang, T. N. Krupenkin, P. Mach and E. A. Chandross, *Adv. Mater.*, 2003, **15**, 940-943.

[24] C.-P. Chiu, T.-J. Chiang a, J.-K. Chen, F.-C. Chang, F.-H. Ko, C.-W. Chu, S.-W. Kuo, and S.-K. Fan, *J. Adhesion Sci. Technol.*, 2012, **26**, 1773–1788.

[25] Z. Wan, H. Zeng and A. Feinerman, *Appl. Phys. Lett.*, 2006, **89**, 201107.

[26] L. Hou, N. R. Smith, and J. Heikenfeld, *Appl. Phys. Lett.*, 2007, **90**, 251114.

[27] D.-G. Lee, J. Park, J. Bae, and H.-Y. Kim, *Lab Chip*, 2013,**13**, 274-279.

[28] J. Cheng, S. Park, C.-L. Chen, *Solar Energy*, 2013, **89**, 152-161.

[29] R. A. Hayes and B. J. Feenstra, *Nature*, 2003, **425**, 383-385.

[30] J. Heikenfeld, K. Zhou, E. Kreit, B. Raj, S. Yang, B. Sun, A. Milarcik, L. Clapp, and R. Schwartz, *Nature Photonics*, 2009, **3**, 292-296.

[31] W. C. Nelson and C.-J. Kim, *J. Adhesion Sci. Technol.*, 2012, **26**, 1747-1771.

[32] F. Mugele and J.-C. Baret, *J. Phys.: Comdens. Matter*, 2005, **17**, R705-R774.

[33] A. W. Adamson and A. P. Gast, *Physical Chemistry of Surfaces*, Wiley, New York USA, 1997.

[34] B. Berge, *C. R. Acad. Sci. II*, 1993, **317**, 157-163.

[35] M. Vallet, M. Ballade, and B. Berge, *Eur. Phys. J. B*, 1999, **11**, 583-591.

[36] T. B. Jones, M. Gunji, M. Washizu, and M. J. Feldman, *J. Appl. Phys.*, 2001, **89**, 1441-1448.

[37] S.-K. Fan, T.-T. Wang, P.-W. Huang, and Y.-H. Peng, *Lab Chip*, 2008, **8**, 1325-1331.

[38] P. S. Drzaic, *Liquid Crystal Dispersions*, World Scientific, Singapore, 1995.

[39] S.-K. Fan, C.-P. Chiu, and J.-W. Lin, *Appl. Phys. Lett.*, 2009, **94**, 164109.

[40] H. A. Pohl, *Dielectrophoresis*, Cambridge University Press, Cambridge UK, 1978.

[41] H. Morgan and N. G. Green, *AC Electrokinetics: colloids and nanoparticles*, Research Studies Press Ltd., Baldock UK, 2003.

[42] T. B. Jones, *Electromechanics of Particles*, Cambridge University Press, Cambridge UK, 1995.

[43] S.-K. Fan, C.-P. Chiu, and P.-W. Huang, *Biomicrofluidics*, 2010, **4**, 043011.

[44] S.-K. Fan, C.-P. Chiu, C.-H. Hsu, S.-C. Chen, L.-L. Huang, Y.-H. Lin, W.-F. Fang, J.-K. Chen, and J.-T. Yang, *Lab Chip*, 2012, **12**, 4870-4876.

[45] B. Comiskey, J. D. Albert, H. Yoshizawa and J. Jacobson, *Nature*, 1998, **394**,

253-255.

[46] S. K. Chung, K. Rhee, and S. K. Cho, *Int. J. Precis. Eng. Manuf.*, 2010, **11**, 991-1006.

[47] Y. Zhao and S. K. Cho, *Lab Chip*, 2007, **7**, 273-280.

[48] S.-K. Fan and D.-Y. Lin, *International Journal of Automation and Smart Technology*, 2012, **2**, 69-74.

[49] H. Pellat, *C. R. Acad. Sci. Paris*, 1895, **119**, 691-694.

[50] J. R. Melcher and M. Hurwitz, *J. Spacecr. Rockets*, 1967, **4**, 864-871.

[51] C.-C. Cheng, C. A. Chang, J. A. Yeh, *Opt. Express*, 2006, **14**, 4101-4106.

[52] S.-K. Fan, Y.-W. Hsu, and C.-H. Chen, *Lab Chip*, 2011, **11**, 2500-2508.

[53] S.-K. Fan, Y.-T. Shen , L.-P. Tsai, C.-C. Hsu, F.-H. Ko, and Y.-T. Cheng, *Lab Chip*, 2012, **12**, 3694-3699.

[54] M. A. Lieberman and A. J. Lichtenberg, *Principles of Plasma Discharges and Materials Processing*, Wiley, New York USA, 1994.

Table 1 Manipulation on the EMF platform.

Principle	Object	Result	Figure and reference	Note of parameters
Electrowetting with V_D	Water droplet in air on PDLC	PDLC transmittance	Fig. 2(f)-2(i)[39]	1 kHz, 100 V_{RMS} for a 300 μm-high 0.75 μL water droplet
	Cell and particle suspension droplet in oil	Moving a water droplet in a medium or in an oil shell and thus altering local optical properties (e.g., refractive index)	Fig. 3 (k) and 3(m)[37]	1 kHz, 80 V_{RMS} for a 200 μm-high 0.5 μL sucrose solution droplet with cells (8.6×10^5 /mL) or a water droplet with 5 μm particles (1.4×10^8/mL) in 50 cSt silicone oil
	Particle suspension droplet in air		Fig. 4 (f) and 4(g)[43]	1 kHz, 50 V_{RMS} for 100 μm-high 0.1 μL water droplet with 5 μm particle (1.4×10^8/mL) in air
	Water and encapsulated droplets (1:1 W/O)		Fig. 5(e) and 5(f)[18]	1 kHz, 34 V_{RMS} for a 25 μm-high 25 nL water droplet in air or in a 25 nL silicone oil (20 cSt) shell
	Water, encapsulated (10:1 W/O), and water droplets in organic solution		Fig. 5(g)-5(j)[52]	1 kHz, 48 V_{RMS} for a 25 μm-high 25 nL water droplet in air, in a 2.5 nL silicone oil (10 cSt) shell, or in hexane
Particle dielectrophoresis and polarization with V_L	Cell and particle in droplet	Cell/particle location	Fig. 3(h)-3(m)[37]	2 MHz, 60 V_{RMS} for a 25 μm-high 0.5 μL sucrose solution droplet with cells (8.6×10^5 /mL) or a water droplet with 5 μm particles (1.4×10^8/mL) in silicone oil (50 cSt)
	Particle in water	Transmittance and reflectance	Fig. 4(c), 4(d), 4(f), and 4(g)[43]	200 kHz, 28 V_{RMS} and 50 V_{RMS} for a 100 μm-high particle suspension (5 μm, 1.4×10^8/mL) in water
			Fig. 4(i)-4(m)[44]	500 kHz, 48 V_{RMS} and 9 V_{RMS} for a 100 μm-high particle suspension (3 μm, 1.68×10^9/mL) in water
Liquid dielectrophoresis with V_L	Oil droplet in air	Moving oil droplet or bubble and thus altering local optical properties (e.g., refractive index)	Fig. 5(b) and 5(c)[18]	420 V_{DC} for a 75 μm-high 0.15 μL silicone oil (20 cSt) droplet in air
			Fig. 5(e)[18]	260 V_{DC} for a 25 μm-high 25 nL silicone oil (20 cSt) droplet in air
			Fig. 5(g)[52]	240 V_{DC} for 25 μm-high 2.5 nL silicone oil (10 cSt) droplet in air
	Bubble in oil		Fig. 6(c)-6(f)[53]	2.4 kHz, 315 V_{RMS} for a 50 μm-high 200 nL Ar, He, and Ar/He mixture bubble in silicone oil (20 cSt)
	Bubble microplasma in oil	Emission	Fig. 6(j) and 6(k)[53]	2.4 kHz, 655 V_{RMS} for a 50 μm-high 200 nL Ar bubble microplasma in silicone oil (20 cSt)

Captions of figures

Fig. 1 Basic electrowetting phenomenon and the EMF platform. (a) Electrowetting in the sessile-drop experiment. (b) Electrowetting on an open surface device. (c) Electrowetting between parallel plates. (d) EMF platform driving droplets with patterned electrodes between parallel plates.

Fig. 2 EMF platform using a solid electro-optical dielectric layer, PDLC[39]. (a) and (b) Electrowetting with reorientation of LC droplets within the PDLC layer. (c) and (d) Electrowetting-driven liquid lens using PDLC as dielectric layer. (e) Cross section and top view of the EMF platform demonstrating droplet manipulation with PDLC. (f) and (g) Droplet transport. (h) and (i) Droplet splitting. Reproduced with permission from *Appl. Phys. Lett.*, 2009, **94**, 164109. Copyright 2009, AIP Publishing LLC.

Fig. 3 Particle manipulation by dielectrophoresis on the EMF platform[37]. (a) and (b) Non-uniform electric field in a droplet provided on applying V_{HF} on strip electrodes. (c) and (d) Top view and cross section of the EMF platform. (e)-(g) Driving procedure for particle and cell concentration: V_{HF} drives particles by dielectrophoresis; V_{LF} drives droplets by electrowetting. (h)-(k) Concentrating mammalian cells (Neuro-2a). (l) and (m) Concentrating polystyrene particles. Reproduced from *Lab Chip*, 2008, **8**, 1325, with permission from The Royal Society of Chemistry.

Fig. 4 Light regulation on modulating liquid transmittance based on formation of particle chains[43,44]. (a) and (b) A uniform electric field forms particle chains of a suspension droplet. (c) and (d) Variation of reflectance of a droplet between parallel electrodes. (e) Driving droplets with V_{LF} and particles with V_{HF}. (f) and (g) Altering positioning and reflectance of a suspension droplet on electrowetting (V_{LF}) and dielectrophoresis (V_{HF}), respectively. (h) Cross section of reflective electronic display based on formation of a particle chain with directly driven and arrayed electodes. (i) and (j) Display medium with blue and red polystyrene particles driven on applying an electric field on the directly driven electrode 'NCTU CPT'. (k)-(m) A display medium with black polystyrene particles driven on a 5 × 5 electrode array. Reproduced with permission from *Biomicrofluidics*, 2010, **4**, 043011. Copyright 2010, AIP Publishing LLC. Reproduced from *Lab Chip*, 2012, **12**, 4870, with permission from The Royal Society of Chemistry.

Fig. 5 EMF platform capable of driving conductive (water) and dielectric (oil) droplets[18,52]. (a) Liquid dielectrophoresis drives a dielectric droplet of greater relative permittivity into the region of smaller relative permittivity (e.g., air). (b) and (c) Silicone oil droplet manipulations. (d) Manipulating oil and water droplets with dielectrophoresis and electrowetting, respectively. (e) Driving oil (top) and water (bottom) droplets. (f) Formation of an encapsulated droplet. (g)-(j) Preparation of an encapsulated droplet with a metered and removable oil shell. Reproduced from *Lab Chip*, 2009, **9**, 1236, and *Lab Chip*, 2011, **11**, 2500, with permission from The Royal Society of Chemistry.

Fig. 6 Bubble and microplasma manipulations on the EMF platform[53]. (a) Cross section and (b) top view of the EMF platform. (c)-(f) Manipulation of Ar, He and Ar/He mixture bubbles. (g) Ignition and actuation of bubble microplasma. (h) and (i) Ignition of Ar microplasma from a gas phase (h) to a plasma phase (i). (j) and (k) Transport of bubble microplasma. (l)-(o) Microplasma splitting. Reproduced from *Lab Chip*, 2012, **12**, 3694, with permission from The Royal Society of Chemistry.

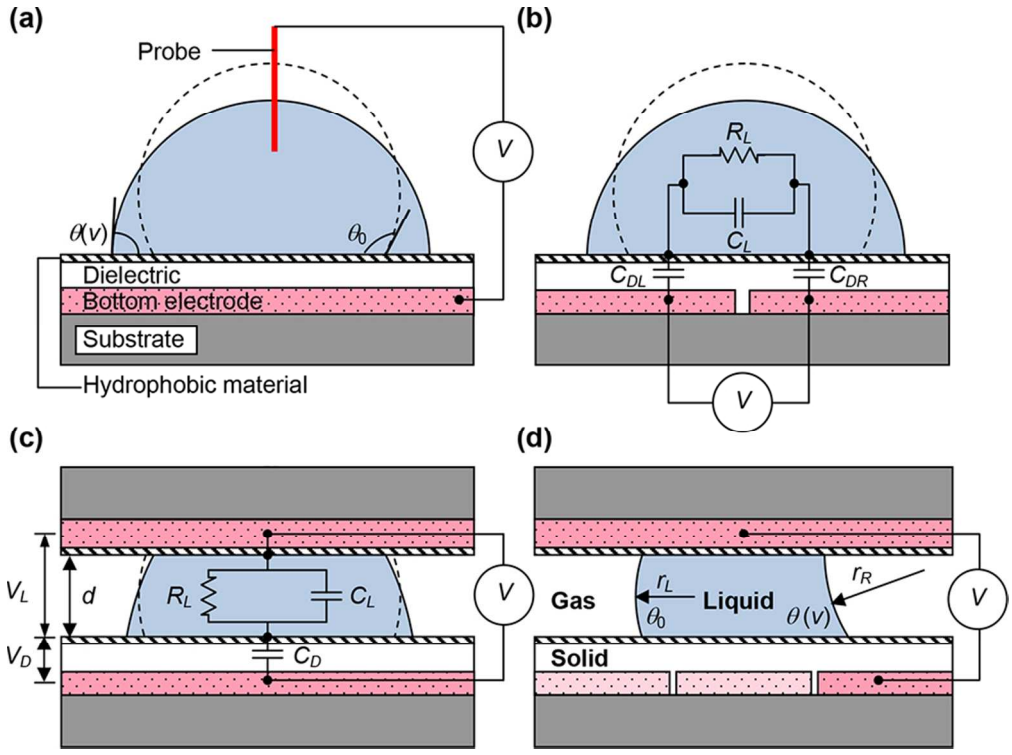

Fig. 1 Basic electrowetting phenomenon and the EMF platform. (a) Electrowetting in the sessile-drop experiment. (b) Electrowetting on an open surface device. (c) Electrowetting between parallel plates. (d) EMF platform driving droplets with patterned electrodes between parallel plates.
82x61mm (300 x 300 DPI)

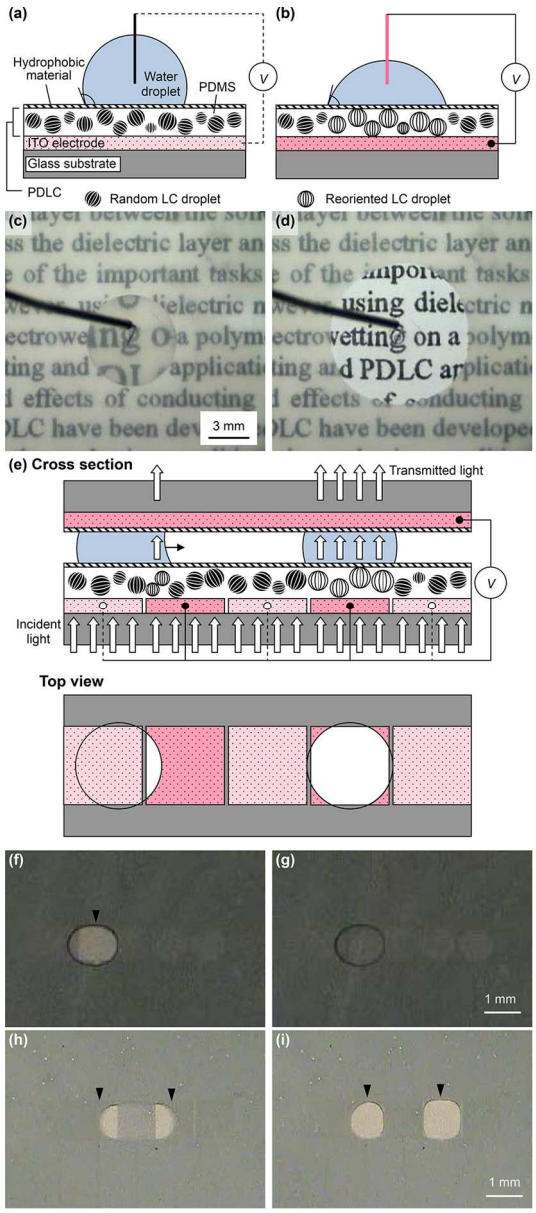

Fig. 2 EMF platform using a solid electro-optical dielectric layer, PDLC39. (a) and (b) Electrowetting with reorientation of LC droplets within the PDLC layer. (c) and (d) Electrowetting-driven liquid lens using PDLC as dielectric layer. (e) Cross section and top view of the EMF platform demonstrating droplet manipulation with PDLC. (f) and (g) Droplet transport. (h) and (i) Droplet splitting. Reproduced with permission from Appl. Phys. Lett., 2009, 94, 164109. Copyright 2009, AIP Publishing LLC.
82x189mm (300 x 300 DPI)

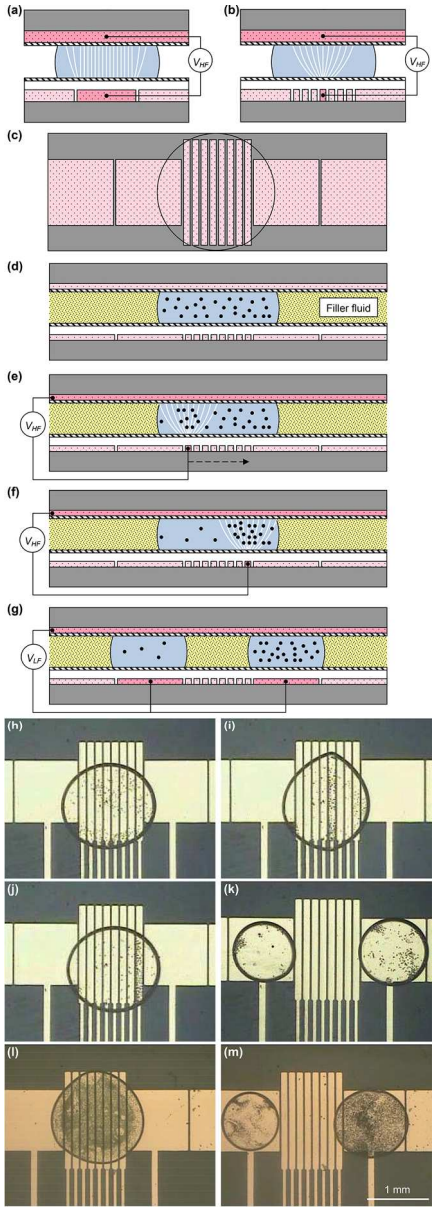

Fig. 3 Particle manipulation by dielectrophoresis on the EMF platform37. (a) and (b) Non-uniform electric field in a droplet provided on applying VHF on strip electrodes. (c) and (d) Top view and cross section of the EMF platform. (e)-(g) Driving procedure for particle and cell concentration: VHF drives particles by dielectrophoresis; VLF drives droplets by electrowetting. (h)-(k) Concentrating mammalian cells (Neuro-2a). (l) and (m) Concentrating polystyrene particles. Reproduced from Lab Chip, 2008, 8, 1325, with permission from The Royal Society of Chemistry.
82x233mm (300 x 300 DPI)

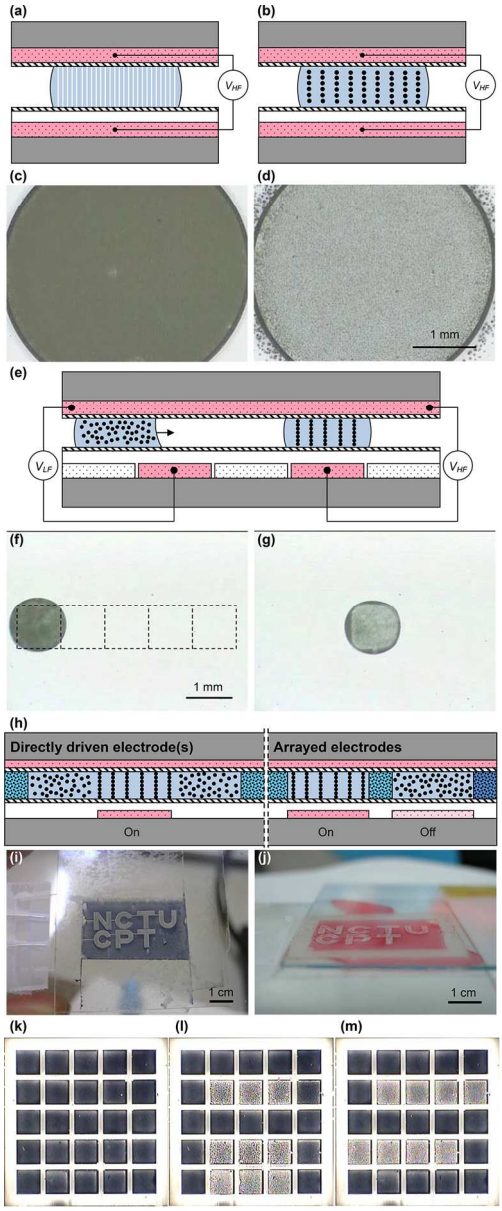

Fig. 4 Light regulation on modulating liquid transmittance based on formation of particle chains43,44. (a) and (b) A uniform electric field forms particle chains of a suspension droplet. (c) and (d) Variation of reflectance of a droplet between parallel electrodes. (e) Driving droplets with VLF and particles with VHF. (f) and (g) Altering positioning and reflectance of a suspension droplet on electrowetting (VLF) and dielectrophoresis (VHF), respectively. (h) Cross section of reflective electronic display based on formation of a particle chain with directly driven and arrayed electodes. (i) and (j) Display medium with blue and red polystyrene particles driven on applying an electric field on the directly driven electrode 'NCTU CPT'. (k)-(m) A display medium with black polystyrene particles driven on a 5 × 5 electrode array. Reproduced with permission from Biomicrofluidics, 2010, 4, 043011. Copyright 2010, AIP Publishing LLC. Reproduced from Lab Chip, 2012, 12, 4870, with permission from The Royal Society of Chemistry.
82x201mm (300 x 300 DPI)

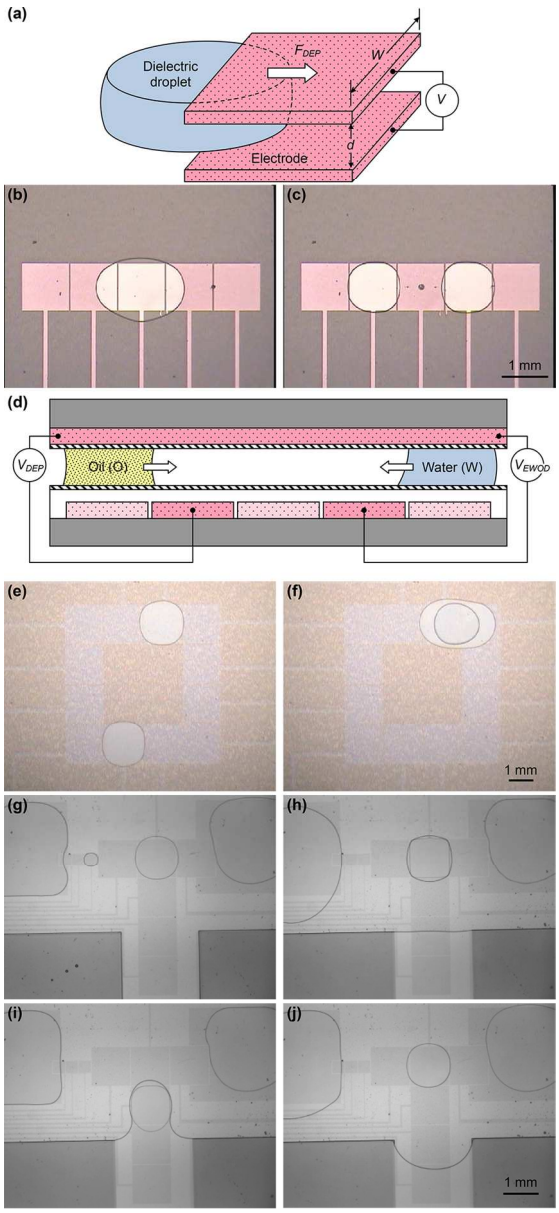

Fig. 5 EMF platform capable of driving conductive (water) and dielectric (oil) droplets18,52. (a) Liquid dielectrophoresis drives a dielectric droplet of greater relative permittivity into the region of smaller relative permittivity (e.g., air). (b) and (c) Silicone oil droplet manipulations. (d) Manipulating oil and water droplets with dielectrophoresis and electrowetting, respectively. (e) Driving oil (top) and water (bottom) droplets. (f) Formation of an encapsulated droplet. (g)-(j) Preparation of an encapsulated droplet with a metered and removable oil shell. Reproduced from Lab Chip, 2009, 9, 1236, and Lab Chip, 2011, 11, 2500, with permission from The Royal Society of Chemistry.
82x180mm (300 x 300 DPI)

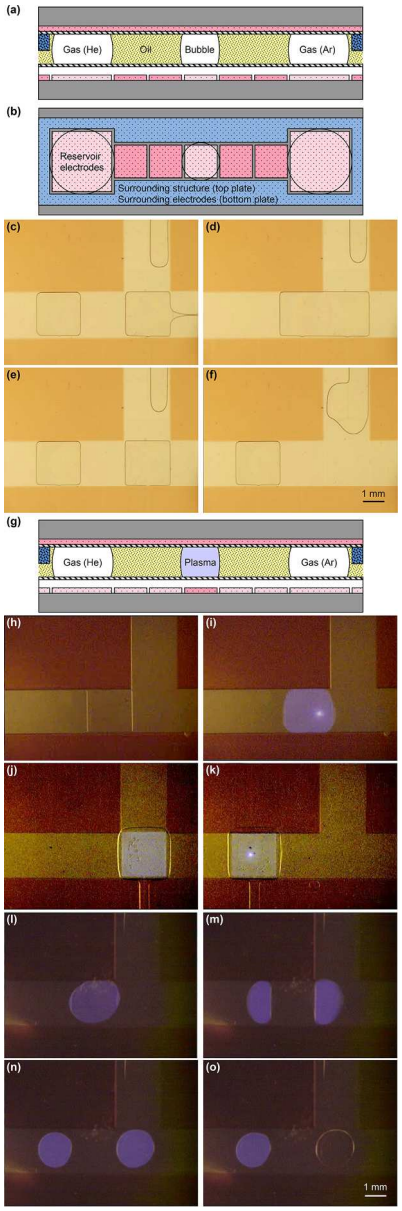

Fig. 6 Bubble and microplasma manipulations on the EMF platform53. (a) Cross section and (b) top view of the EMF platform. (c)-(f) Manipulation of Ar, He and Ar/He mixture bubbles. (g) Ignition and actuation of bubble microplasma. (h) and (i) Ignition of Ar microplasma from a gas phase (h) to a plasma phase (i). (j) and (k) Transport of bubble microplasma. (l)-(o) Microplasma splitting. Reproduced from Lab Chip, 2012, 12, 3694, with permission from The Royal Society of Chemistry.
82x253mm (300 x 300 DPI)